Journal of Alloys and Compounds 495 (2010) 491–494

Contents lists available at ScienceDirect

Journal of Alloys and Compounds

journal homepage: www.elsevier.com/locate/jallcom

Structural and magnetic properties of $Fe_{60}Al_{40}$ alloys prepared by means of a magnetic mill

R. Bernal-Correa[a], A. Rosales-Rivera[a,*], P. Pineda-Gómez[a,b], N.A. Salazar[a]

[a] Laboratorio de Magnetismo y Materiales Avanzados, Facultad de Ciencias Exactas y Naturales, Universidad Nacional de Colombia, Manizales, Colombia
[b] Universidad de Caldas, Manizales, Colombia

ARTICLE INFO

Article history:
Received 10 July 2008
Received in revised form 10 July 2009
Accepted 18 August 2009
Available online 25 August 2009

Keywords:
FeAl alloy
Mechanical alloying
Ball milling
Structural and magnetic properties

ABSTRACT

A study on synthesis, structural and magnetic characterization of $Fe_{60}Al_{40}$ (at.%) alloys prepared by means of mechanical alloying process is presented. The mechanical alloying was performed using a milling device with magnetically controlled ball movement (Uni-Ball-Mill 5 equipment) at several milling times. The characterization was carried out via X-ray diffraction (XRD), scanning electron microscopy (SEM) and vibrating sample magnetometer (VSM). The effects of milling time on the structural state, morphological evolution and magnetic behaviour of the $Fe_{60}Al_{40}$ (at.%) alloys are discussed. Besides, in this current study we emphasize the result that indicating a ferro-para-ferromagnetic transition from a correlation between X-ray diffraction and magnetization data.

1. Introduction

Since its development in the 1970s, the mechanical alloying [1] has become one of the most common techniques used to produce nanostructured intermetallic materials due to its versatility and relatively low cost [2]. In this context, ball mills are used for mechanical alloying in which they are not only used for grinding but for cold welding as well, with the goal of producing alloys from powders. There are many types of ball mills such as the planetary mills [3] and the Uni-Ball-Mill [4], each having its specific properties and advantages. Among the intermetallic materials prepared using mechanical alloying process is the iron–aluminum ($Fe_{1-x}Al_x$) compound which has been largely studied in the last four decades due to their excellent functional properties, both magnetic [5,6] and structural [7]. This compound has been prepared by means of several techniques including, cold working procedures [8], mechanical alloying [9,10], and ion irradiation [11]. As it is known [12], in the $Fe_{1-x}Al_x$ compound, the room temperature ferromagnetic state of the atomically ordered alloy gradually disappears with increasing Al content, as expected from dilution models, up to $x \leq 0.2$. On further increasing x, the ferromagnetic state disappears more rapidly, becoming paramagnetic for alloys with $x > 0.32$. However, atomic ordered $Fe_{1-x}Al_x$ alloys with $x > 0.32$ can become ferromagnetic, at room temperature, after being disordered (i.e. atomically intermixed) [12]. In this work, the $Fe_{60}Al_{40}$ (at.%) alloy is prepared using an Uni-Ball-Mill 5 device, in which it is feasible to control the nature and magnitude of impact of balls by controlling the magnetic field strength with help of adjustable magnets [4]. In this device, the basic mechanism involved during the developing of the mechanical alloying process can be described like a succession of several steps of fracture and welding, produced during impact and friction, resulting in an atomic reorganization and intermixing.

2. Experimental method

$Fe_{60}Al_{40}$ (at.%) alloys were produced from iron and aluminum powder precursors (99.9% purity), using an Uni-Ball-Mill 5.0 device with a hardened steel vial of 8 and 10 cm of inner and outer diameter, respectively, and stainless steel balls of 8 mm diameter. A 2% of ethilbiesteramide (EBS) powder wax was used as an agent to control the process [13]. Powders were separately weighted in order to obtain the desired composition. Sample mass was calculated by ball-to-powder mass ratio 20:1. The milling process was carried out in low vacuum (10^{-2} mbar) in shearing and impact modes [4]. In shearing mode, the magnet is placed at the bottom about 1 cm from the vial during 2 h. During this time, the rotation was maintained at 20 rpm. Then was selected the impact mode, in which the magnet is placed at the bottom close to the vial—magnet in position 3 O'clock—for different intervals of time (t = 0, 2, 4, 8, 30, 50 and 100 h). In this case, the rotation was maintained at 175 rpm. The structural state was determined by XRD using a Rigaku Miniflex II diffractometer with Cu Kα radiation (λ = 1.54056 Å) in the $20 \leq 2\theta \leq 100$ range at steps of 0.02 s^{-1}. The XRD patterns were refined using the Rietveld method with a pseudovoight type program. Alloying evolution was observed in backscattered electrons mode using a FEI XL30 New Look scanning electron microscopy (SEM) equipped with an energy dispersive spectroscopy (EDX) facility. The magnetic field (H) dependence of magnetization (M) was measured using a home-made Foner-type vibrating sample magnetometer (VSM), in the field range $-6 \leq H \leq 6$ kOe, at room temperature. The VSM was calibrated using a nickel sample and magnetization data were obtained for consecutive H-steps, stabilizing H before each reading.

* Corresponding author.
E-mail address: arosalesr@unal.edu.co (A. Rosales-Rivera).

0925-8388/$ – see front matter © 2009 Elsevier B.V. All rights reserved.
doi:10.1016/j.jallcom.2009.08.085

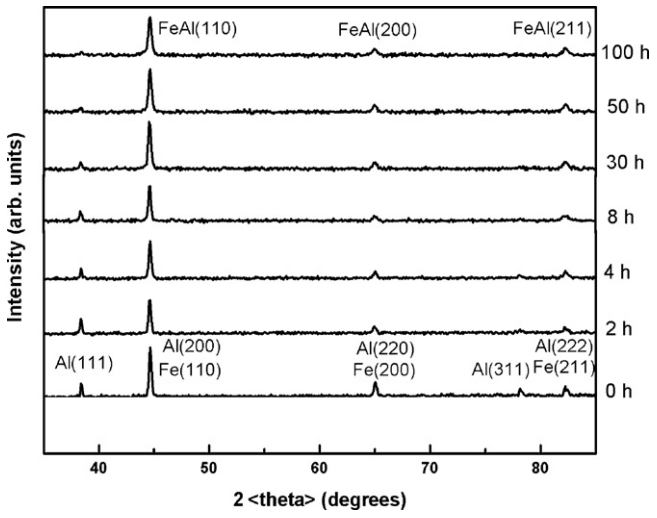

Fig. 1. XRD patterns of $Fe_{60}Al_{40}$ (at.%) alloys for several milling times.

3. Results and discussion

The XRD patterns of the $Fe_{60}Al_{40}$ (at.%) samples for several milling times are shown in Fig. 1. The unmilled sample ($t = 0$ h) exhibits a pattern consistent with both an Al and Fe precursors structure, where the Al (2 0 0), (2 2 0) and (2 2 2) peaks overlap with the Fe (1 1 0), (2 0 0) and (2 1 1) peaks, respectively. On milling, the intensity of the Al (1 1 1) and (3 1 1) peaks decreases with increasing of milling time. On further increasing milling time, the Al (3 1 1) peak completely disappears as it does for $t = 30$ h while that the Al (1 1 1) peak gradually disappears and the FeAl (1 1 0) peak becomes the most intense in the XRD patterns. The milling time dependence of the intensity of the Al (1 1 1) peak is shown in Fig. 2. The features described above reflect the replacement of the separate Fe and Al phases by a solid solution (FeAl phase), which occurs for long milling times. This result is in agreement with the variation in the intensity of Al peaks in FeAl alloys reported by Refs. [14–17]. In Ref. [14], the disappearance of the Al peaks mentioned above was associated with the migration of Al into Fe, indicating the formation of an intermetallic FeAl alloy. Another long milling time feature evidenced in Fig. 1, is the broadening of the FeAl (1 1 0) peak. The broadening of XRD peaks is associated with both crystallite size refinement and increase of micro strains presents in the alloy. As it

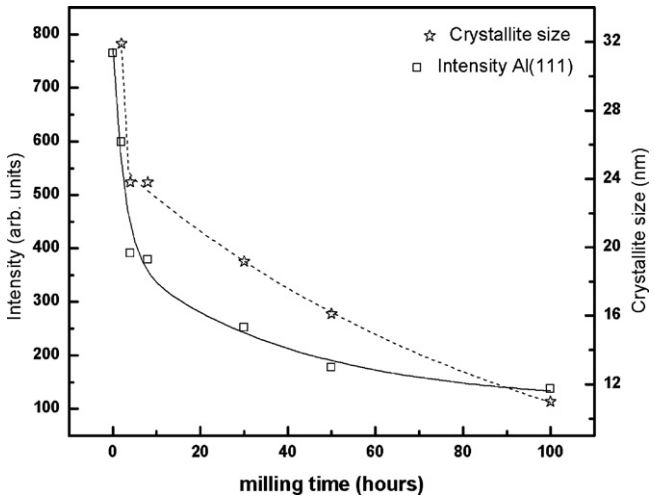

Fig. 2. Milling time dependence of the crystallite average size.

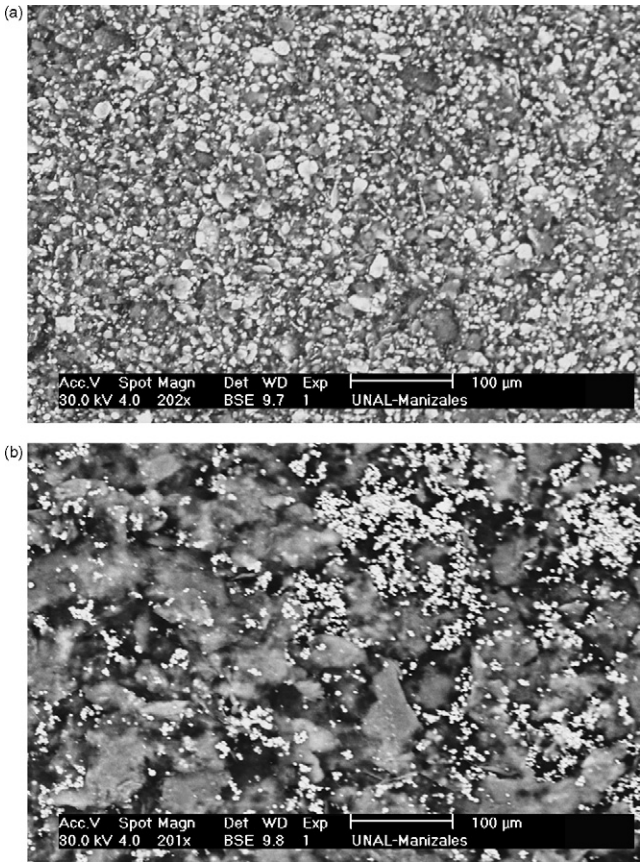

Fig. 3. a SEM micrographs of $Fe_{60}Al_{40}$ (at.%) alloys for milling time equal to 0 h. b SEM micrographs of $Fe_{60}Al_{40}$ (at.%) alloys for milling time equal to 30 h.

is well known, the mechanical alloying process involves a decrease in crystallite size [1]. An analysis of the evolution of the micro structural refinement of the crystallite size, d, and the micro strain, ε, could be performed using the Williamson–Hall [18] method, $(B_{exp} - B_{eq})^{1/2} \cos\theta = \varepsilon \sin\theta + (0.9\lambda/d)$, where B_{exp} is the broadening obtained from diffraction peaks, B_{eq} is the instrumental broadening obtained from an X-ray pattern of standard silicon sample used for instrumental calibration (in the present case, $B_{eq} = 0.173^{\circ}$), and λ is the wavelength of the Cu Kα radiation. It is important to remark that the crystallite size determined by XRD provides average coherently diffracting domain sizes. The milling time dependence of the crystallite average size obtained from FeAl (1 1 0), (2 0 0), and (2 1 1) peaks and with aid of the Williamson–Hall expression is shown in Fig. 2, where it is observed that d decreases initially very rapidly, from 32 up to 24 nm corresponding to milling times of $t = 0$ and 4 h, respectively. Then d proceeds more gradually and reaches a value equal to 11 nm for $t = 100$ h. This behaviour indicates that a mechanism of welding and subsequent breaking is present in the formation of FeAl alloys under studied and is also compatible with studies previously reported [19] on FeAl alloys. This result is also in agreement with the evolution of the crystallite size with the milling time in a FeAl(40%) alloy prepared by means of a planetary mill [9]. The crystallite size reduction becomes these materials of interest both from basic and technological points of view because the crystallite size reduction up to monodomain eliminates the influence of magnetic domain walls [20]. On the other hand, the obtained micro strain level values during the mechanical alloying process ranged from 6×10^{-3} at $t = 4$ h to 15×10^{-3} at $t = 100$ h. The morphological evolution of the FeAl alloys corresponding to milling times, $t = 0$ and 30 h, obtained by SEM, is shown in Fig. 3a and b. For $t = 0$ h (unmilled sample) the presence of small particles of iron (dark

Table 1
Chemical composition of alloys determined using EDX in function of milling time.

Milling time (h)	0	30	50
O (at.%)	0.8	4.6	4.2
Al (at.%)	71.6	44.6	35.2
Fe (at.%)	27.6	50.8	60.6

regions) and aluminum (light regions) is clearly observed (Fig. 3a). For higher milling time (t = 30 h), however, intensive fracturing and welding make most crystallites exhibit a placket or rounded shape and regions where substitution of Al in Fe has taken place are most commonly found, as shown in Fig. 3b. Thus the mechanical alloying process evolves to form the FeAl alloy. However, the presence of Al particle aggregates (light colour and small diameter), iron (dark colour) and FeAl crystallites (gray colour) can be noticed, which can indicate that the alloying process is not complete yet. In addition, the atomic amounts of Fe and Al present in alloy under study were determined using EDX for several milling times and the results are presented in Table 1. As it is shown, contaminant elements such as the oxygen are in minimum proportion which indicates that the materials preparation technique used in this work is a relatively clean one.

The magnetic field (H) dependence of the magnetization (M) for several milling times is shown in Fig. 4. The M *vs*. H curves are those typical of a predominant ferromagnetic state taking place at room temperature. However, the room temperature ferromagnetic state of alloy disappears gradually with increasing milling time. On further increasing milling time, the ferromagnetic state disappears more rapidly as it does for t = 30 h. This characteristic reflects the gradual development of alloying process of Fe with Al. Al reduces the direct ferromagnetic interaction between Fe–Fe sites. As Al content increases during the process of formation of the alloy, an antiferromagnetic super-exchange interaction between Fe sites mediated by Al atoms could takes place in it [21]. However, on increasing milling time even more, the ferromagnetic state is recovered. It could be associated with a disordering (i.e. atomic intermixing) process [12] that occurs in the alloy for long milling times. Several studies sustains that the ferromagnetism in $Fe_{60}Al_{40}$ (at.%) alloys has a two-fold origin including, nearest-neighbor magnetism, named as local environment model [22–24], and changes in the band structure of the material induced by changes in the lattice cell parameter [23–26]. It has been calculated [27], that the total magnetic moment for completely disordered $Fe_{60}Al_{40}$ (at.%) alloy is 108.3 emu/g. Also, a value of saturation magnetization, M_s = 75 emu/g, has been measured [28] in $Fe_{60}Al_{40}$ (at.%). It can be noted by inspection of data of Fig. 4 that the saturation magnetization value determined by extrapolation the linear part of the magnetization curve in high magnetic fields to zero field tends to 11 emu/g and 125 emu/g at t = 30 and 100 h, respectively. A comparison of saturation magnetization values determined above with calculated ones allows us to infer that FeAl alloy is not completely disordered at t = 30 h while that at t = 100 h it is predominantly disordered. It has been observed [29] that good bulk magnetic properties in alloys demand a complete coupling of all the magnetic grains in the sample implying that the ferromagnetic exchange length, L_o, must be greater than crystallite average size, d. In the present study, for $0 < t < 30$ h, both M_s and d decrease with increasing of t; M_s reaches a minimum value equal to 11 emu/g at t = 30 while that d is equal to 19 nm which results larger than L_o and the alloy becomes paramagnetic. Further milling does increase M and decrease d; the latter reaches a value d = 11 nm for t = 100 h which results less than or equal to L_o and the alloy becomes ferromagnetic again. On the other hand, the unsaturated nature of the M *vs*. H curves could be associated to some paramagnetism of the alloys which could leads to high saturation magnetization values. Also, the increase in saturation magnetization with increasing milling time from t = 30 h could be ascribed to Fe contamination from milling media and oxidation of Al.

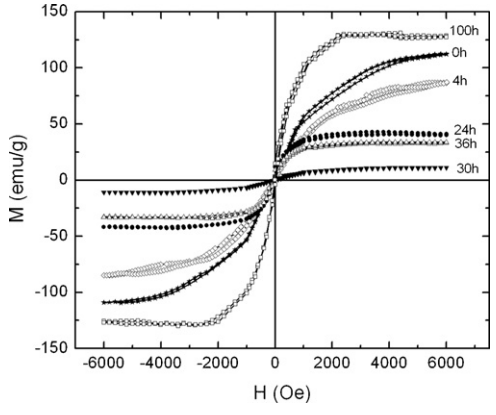

Fig. 4. Magnetic field dependence of the magnetization of $Fe_{60}Al_{40}$ (at.%) alloys for several milling times.

4. Conclusions

We have made a comparative study of the structural, morphological and magnetic properties in $Fe_{0.60}Al_{0.40}$ (at.%) alloys prepared by means of a magnetic mill, which distinguishes the features associates with the moderate and long milling time regimes in this compound. For moderate milling time ($t \leq 30$ h), our XRD, SEM and magnetization results are compatible with the development of an atomically ordered ferromagnetic intermetallic FeAl alloy but its ferromagnetic state disappears gradually with increasing milling time. On further increasing milling time, the ferromagnetic state disappears more rapidly as it does for t = 30 h. For long milling time ($t > 30$ h), however, the ferromagnetic state is recovered which could be associated to an atomic intermixing process.

Acknowledgements

We thank Professor O.H. Giraldo and Professor P.J. Arango by X-ray diffraction and SEM studies, respectively. This work was supported by DIMA-Universidad Nacional de Colombia, Sede Manizales.

References

[1] J.S. Benjamin, Metall. Trans. 1 (1970) 2943;
J.S. Benjamin, Sci. Am. 234 (1976) 40.
[2] G. Principi, Hyper. Interact. 134 (2001) 53.
[3] H. Bakker, G.F. Zhou, H. Yang, Prog. Mater. Sci. 39 (1995) 159.
[4] A. Calka, A.P. Radlinski, Mater. Sci. Eng. A A134 (1991) 1350–1360.
[5] J.H. Westbrook, R.L. Fleischer (Eds.), Properties and Applications of Intermetallic Compounds: Magnetic, Electrical and Optical, vol. 4, Wiley, New York, 2000.
[6] M.M. Rico, J.M. Greneche, G.A. Pérez Alcázar, J. Alloys Compd. 398 (2005) 26–32.
[7] J.H. Westbrook, R.L. Fleischer (Eds.), Properties and Applications of Intermetallic Compounds: Structural Applications, vol. 3, Wiley, New York, 2000.
[8] J. Sort, A. Concustell, E. Menéndez, S. Suriñach, K.V. Rao, S.C. Deevi, M.D. Baró, J. Nogués, Adv. Mater 18 (2006) 1717.
[9] S. Gialanella, X. Amils, M.D. Baró, P. Delcroix, G. Le Caër, L. Luterotti, S. Suriñach, Acta Mater. 46 (9) (1998) 3305–3316.
[10] R.A. Varin, J. Bystrzycki, A. Calka, Intermetallics 7 (1999) 917–930.
[11] J. Fassbender, M.O. Liedke, T. Strache, W. Möller, E. Menéndez, J. Sort, K.V. Rao, S.C. Deevi, J. Nogués, Phys. Rev. B 77 (2008) 174430.
[12] A. Taylor, R.M. Jones, J. Phys. Chem. Solids 6 (1958) 16.
[13] S. Suryanarayana, Prog. Mater. Sci. 46 (2001) 1–148.
[14] S. Enzo, R. Frattini, R. Gupta, P.P. Macri, G. Principi, L. Schiffini, G. Scipioni, Acta Mater. 44 (1996) 3105.
[15] E. Bonetti, S. Enzo, G. Principi, L. Schiffini, in: C. Suryanarayana, J. Singh, F.H. Froes (Eds.), Processing and Properties of Nanocrystalline Materials, Metallurgical Society of AIME, Warrendale, PA, 1996, p. 153.
[16] F. Cardellini, V. Contini, R. Gupta, G. Mazzone, A. Montone, A. Perin, G. Principi, J. Mater. Sci. 33 (1998) 2519–2527.

[17] V. Sebastian, N. Lakshmi, K. Venugopalan, Intermetallics 15 (2007) 1006–1012.
[18] G.K. Williamson, W.H. May, Acta Metall. 1 (1953) 22.
[19] K. Wolsky, G. Le Caer, P. Delcroix, R. Fillit, F. Thevenot, J. Le Coze, Mater. Sci. Eng. A 207 (1996) 97.
[20] M. Pękała, D. Oleszak, E. Jartych, J.K. Żurawicz, J. Non-Cryst. Solids 250–252 (1999) 757–761.
[21] J.A. Plascak, L.E. Zamora, G.A. Perez-Alcazar, Phys. Rev. B 61 (2000) 3188–3191.
[22] E. Menéndez, J. Sort, M.O. Liedke, J. Fassbender, S. Suriñach, M.D. Baró, J. Nogués, New J. Phys. 10 (2008) 10 (103030).
[23] P.A. Beck, Metall. Trans. 2 (1971) 2015.
[24] S. Takahashi, J. Magn. Magn. Mater. 54–57 (1986) 1065.
[25] M. Fujii, K. Saito, K. Wakayama, T. Yoshioka, N. Nishio, M. Shiojiri, Philos. Mag. A 79 (1999) 2013.
[26] J. Nogués, et al., Phys. Rev. B 74 (2006) 024407.
[27] Q. Zeng, I. Baker, Intermetallics 14 (2006) 396–405.
[28] X. Amils, J. Nogués, S. Suriñach, J.S. Muñoz, L. Lutterotti, S. Gialanella, M.D. Baró, Nanostruct. Mater. 11 (6) (1999) 689–695.
[29] A. Hernando, J.M. González, Hyper. Interact. 130 (2000) 221.